

Enantioselective Hydroxylation of Benzylic C(sp³)–H Bonds by an Artificial Iron Hydroxylase Based on the Biotin–Streptavidin Technology

Joan Serrano-Plana, Corentin Rumo, Johannes G. Rebelein, Ryan L. Peterson, Maxime Barnet, and Thomas R. Ward*



Cite This: *J. Am. Chem. Soc.* 2020, 142, 10617–10623



Read Online

ACCESS |



Metrics & More



Article Recommendations



Supporting Information

ABSTRACT: The selective hydroxylation of C–H bonds is of great interest to the synthetic community. Both homogeneous catalysts and enzymes offer complementary means to tackle this challenge. Herein, we show that biotinylated Fe(TAML)-complexes (TAML = Tetra Amido Macrocylic Ligand) can be used as cofactors for incorporation into streptavidin to assemble artificial hydroxylases. Chemo-genetic optimization of both cofactor and streptavidin allowed optimizing the performance of the hydroxylase. Using H₂O₂ as oxidant, up to ~300 turnovers for the oxidation of benzylic C–H bonds were obtained. Upgrading the ee was achieved by kinetic resolution of the resulting benzylic alcohol to afford up to >98% ee for (*R*)-tetralol. X-ray analysis of artificial hydroxylases highlights critical details of the second coordination sphere around the Fe(TAML) cofactor.

The selective functionalization of C–H bonds represents one of the frontiers in synthetic methodology.^{1–7} To address this challenge, homogeneous catalysis often relies on directing groups present on the substrate that coordinate to the metal center, thus allowing distinguishing between equally reactive C–H bonds.⁷ Enzymes have been optimized thanks to evolution to differentiate C–H bonds with exquisite selectivity: The active site around the cofactor is tailored to ensure proper orientation of the substrate.

For the hydroxylation of inert C–H bonds, iron-containing enzymes and iron-based homogeneous catalysts occupy a place of choice. They are complementary in many respects. While the former operate under physiological conditions, homogeneous catalysts perform best at low temperature in organic solvents. The reactivity of homogeneous catalysts is often tuned via first-coordination sphere modifications, whereas enzymes rely on secondary sphere interactions.

Iron metalloenzymes catalyze the C–H oxyfunctionalization of hydrocarbons via iron–oxygen species resulting from activation of O₂.^{8–17} The selective hydroxylation of C–H bonds using homogeneous catalysts has been achieved by designing structurally elaborated ligands that provide a tailored cavity around the metal center.^{18–33}

To complement homogeneous catalysts and enzymes, artificial metalloenzymes (ArMs), that result from anchoring an abiotic cofactor within a macromolecular scaffold, have attracted increasing interest in the past years. The well-defined secondary coordination sphere around the cofactor provided by the protein offers fascinating perspectives to optimize both activity and selectivity of the ArMs.^{34–39} In this context several protein scaffolds have proven versatile.³⁴ These include carbonic anhydrase,⁴⁰ hemoproteins,^{41,42} proline oligopeptidase,⁴³ lactococcal multiresistance regulator,⁴⁴ four helix bundles,^{45,46} nitrobindin,⁴⁷ (strept)avidin,^{48–50} etc. In the

context of asymmetric C–H hydroxylation, introduction of a Mn-porphycene cofactor within myoglobin afforded promising ArMs⁵¹ that complement evolved cytochrome P450 enzymes.^{52–54}

Fe(TAML) complexes are a versatile family of iron complexes that typically contain a ferric center tightly bound to a tetraamido macrocyclic ligand.^{55,56} Their reactivity as peroxidase mimics has been extensively studied.^{55,57,58} Some Fe(TAML) complexes hydroxylate hydrocarbons in aqueous media using oxidants such as *t*BuOOH or *m*-CPBA^{56,59–61} or electrochemically.⁶² Thanks to their stability in water, we surmised that Fe(TAML) complexes may allow assembly of an iron-based artificial hydroxylase using the biotin–streptavidin technology. The secondary coordination sphere provided by streptavidin (Sav) may enable enantioselective hydroxylation and minimize the formation of less reactive diiron dimeric species.

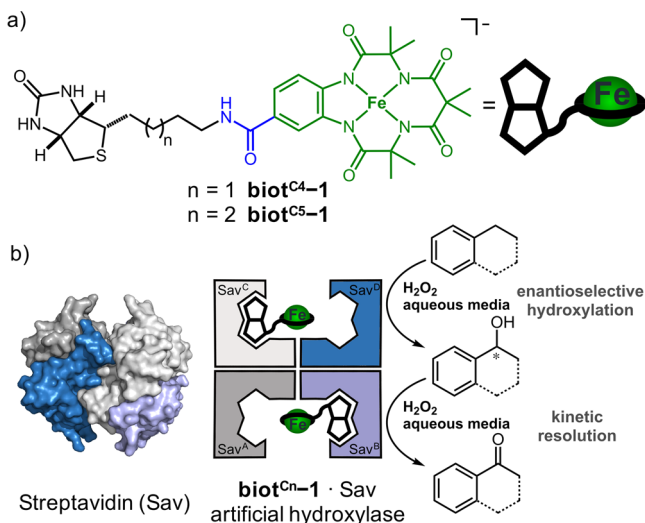
Initial Ligand Design and Reactivity Tests. Sav is a homotetrameric protein that displays exceptional affinity for biotinylated probes (*K*_d 10^{−14} M) and maintains its function and quaternary structure in the presence of various chaotropic agents (pH, temperature, cosolvent tolerance, etc.).^{48,50,63} To ensure localization of the TAML cofactor within Sav, we synthesized a complex bearing a biotin anchor, **biot**^{C5}–1. The anchor was designed to bind to the Fe-TAML moiety through an “inverted” amide bond to the aromatic ring (Scheme 1a) to

Received: March 11, 2020

Published: May 26, 2020

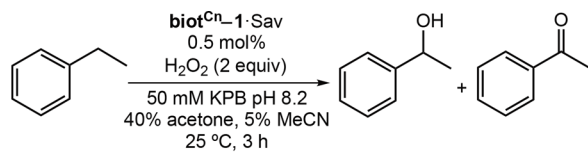


Scheme 1. Artificial C–H Hydroxylase Based on Biotin–Streptavidin: (a) Structure of Cofactors $\text{biot}^{\text{C}4-1}$ and $\text{biot}^{\text{C}5-1}$; (b) Representation of the ArM Resulting from Anchoring $\text{biot}^{\text{C}n-1}$ in Streptavidin



^aTo increase the electron-withdrawing property of the ligand, a biotin amine was coupled to Fe-TAML (green) bearing a carboxylic acid to afford an “inverted” amide (blue).

Scheme 2. Fingerprint Summary of the Artificial Hydroxylase Optimization with PhEt



Sav variant	Cofactor $\text{biot}^{\text{C}n-1}$ C4	C5	Sav variant	Cofactor $\text{biot}^{\text{C}n-1}$ C4	C5
No Sav	○	○	S112G	○	○
WT	○	○	K121A	○	○
S112A	○	○	K121V	○	○
S112L	○	○	K121I	○	○
S112M	○	○	K121M	○	○
S112F	○	○	K121F	○	○
S112Y	○	○	K121W	○	○
S112W	○	○	K121S	○	○
S112T	○	○	K121P	○	○
S112Q	○	○	K121R	○	○
S112R	○	○	K121H	○	○
S112H	○	○	K121D	○	○
S112K	○	○	K121C	○	○
S112E	○	○	S112A/K121L	○	○
S112C	○	○	S112Y/K121R	○	○
S112P	○	○	S112R/K121E	○	○

ee (R) (S)
0 to 5
5 to 10
10 to 15
15 to 20
20 to 25
25 to 30

TTON
5
10
15
20
25
30
35

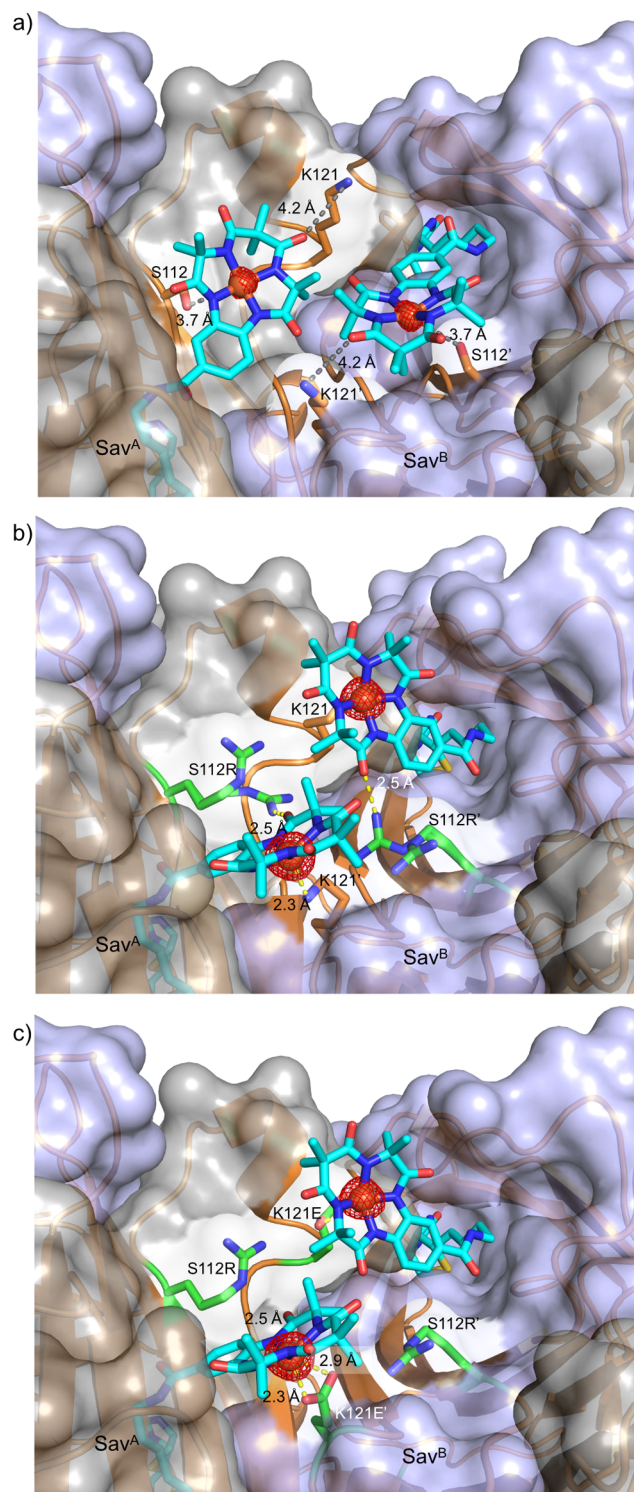


Figure 1. Crystallographic characterization of $\text{biot}^{\text{C}4-1}\cdot\text{Sav}$ WT (a, PDB: 6Y2T), $\text{biot}^{\text{C}4-1}\cdot\text{Sav}$ S112R (b, PDB: 6Y2M), and $\text{biot}^{\text{C}4-1}\cdot\text{Sav}$ S112R/K121E (c, PDB: 6Y25). Sav is depicted as orange cartoon, and its surface representation in gray and mauve (for Sav^A and Sav^B monomers, respectively). The cofactor and relevant amino acids are depicted as sticks. The Fe atoms are depicted as spheres and surrounded by their anomalous electron density (red mesh at 5σ).

increase the electron-withdrawing effect, which has been shown to be beneficial for the reactivity of Fe-TAML complexes.⁶⁴

Table 1. Benzylic C–H Oxidations Catalyzed by $\text{biot}^{\text{C}4}\text{-1}\cdot\text{Sav S112R}^{\text{a}}$

Substrate	TTON	ee (%)	[alcohol] [ketone]	Conversion (%) (alcohol yield (%)) ^c	
	R = CH ₃	57	32	3.2	11.5 (8.8)
	R = CH ₂ CH ₃	26	45	8.4	5.9 (5.3)
	R = (CH ₂) ₂ CH ₃	19	45	7.5	4.3 (3.8)
	R = C(CH ₃) ₂	0	-	-	-
	n = 2	316	65	5.7	60 (44.3)
	300 ^b	>98	1.1	86.8 (34.3)	
	n = 1	205	47	7.4	45.7 (40.2)
	173 ^b	80	0.8	55.7 (24.7)	
	R = OCH ₃	120	12	5.9	26.3 (22.5)
	R = Cl	20	14	3.8	4.1 (3.3)
	R = Br	9	18	>20	2.3 (2.3)

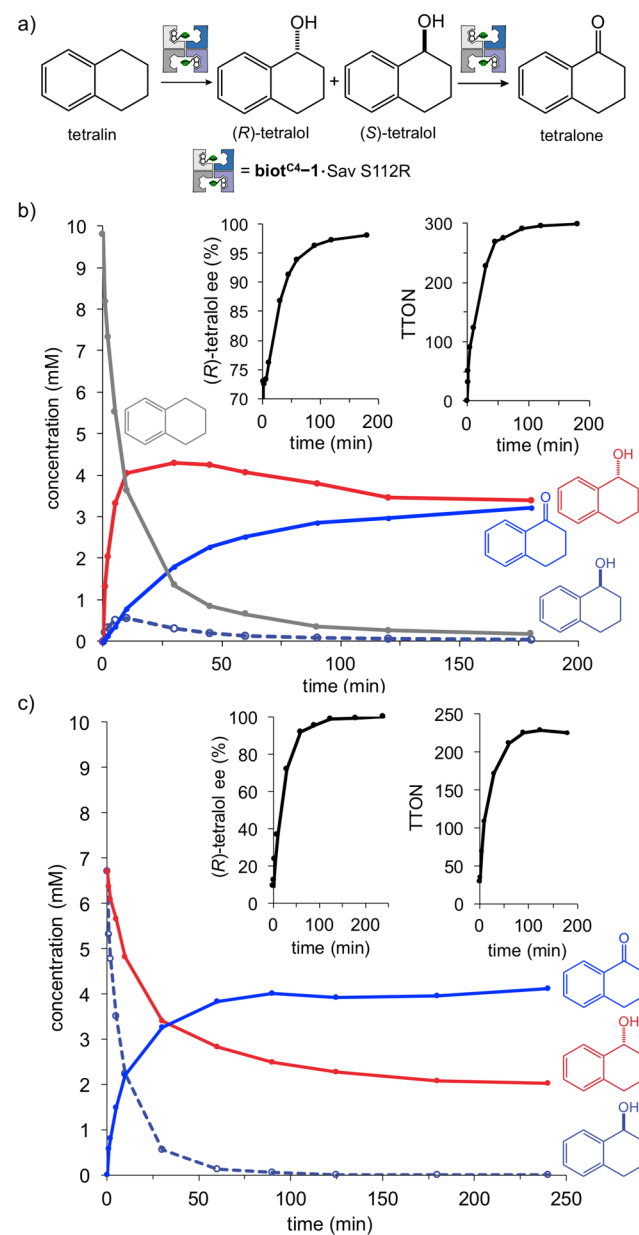
^aConditions: 25 μM $\text{biot}^{\text{C}4}\text{-1}\cdot\text{Sav S112R}$ (50 μM Fe), 20 mM substrate, 20 mM H₂O₂, 50 mM KPB pH 8.5, 35% acetone, 2.5% MeCN, 3 h at 25 °C. ^b10 mM substrate, 25 mM H₂O₂, to promote alcohol overoxidation which yields increased ee. ^cSee Table S6 for more details.

Initial reactivity tests were performed with ethylbenzene (PhEt, BDE_{C–H} = 87 kcal/mol) using 2 equivalents of H₂O₂ in phosphate buffer (KPB) at pH 8.2 and 40% acetone for 3 h.^{61,65} Under these conditions, $\text{biot}^{\text{C}5}\text{-1}\cdot\text{Sav WT}$ afforded (*rac*)-1-phenylethanol ((*rac*)-PhEtOH) and acetophenone (total turnover number, TTON,⁶⁶ = 23). Both activity and selectivity of $\text{biot}^{\text{C}5}\text{-1}\cdot\text{Sav WT}$ were comparable to the free cofactor $\text{biot}^{\text{C}5}\text{-1}$ (TTON = 21, (*rac*)-PhEtOH). Next, we screened a Sav library that included mutations at positions Sav S112X and/or Sav K121X (Scheme 2 and Table S4). The TTON and enantioselectivity remained moderate (up to 16% ee (*R*)-PhEtOH and TTON = 29). We hypothesized that the moderate influence of the host protein on the catalytic performance may be due to the poor localization of the Fe-TAML within the biotin-binding vestibule. We surmised that a shorter biotin Cⁿ-linker may increase the influence of Sav on the catalytic performance by positioning the metal center deeper within the binding pocket. We prepared $\text{biot}^{\text{C}4}\text{-1}$ and evaluated its performance (Schemes 1, 2 and Table S4).

Shortening the Cⁿ-linker positively affects the selectivity: $\text{biot}^{\text{C}4}\text{-1}\cdot\text{Sav WT}$ affords 6% ee (*R*)-PhEtOH. Screening the above Sav library with $\text{biot}^{\text{C}4}\text{-1}$ reveals that close-lying amino acids influence the ee: $\text{biot}^{\text{C}4}\text{-1}\cdot\text{Sav S112R}$ yields 28% ee (*R*)-PhEtOH (TTON = 28), and $\text{biot}^{\text{C}4}\text{-1}\cdot\text{Sav S112R/K121E}$ affords 24% ee (*S*)-PhEtOH (TTON = 29).

Intrigued by these findings, the oxidation of PhEt by $\text{biot}^{\text{C}4}\text{-1}\cdot\text{Sav S112R}$ was monitored. Two consecutive oxidation steps take place. Initially, hydroxylation of the benzylic position affords (*R*)-PhEtOH with ee >40% after a few TTONs (Figure S8). As the reaction progresses, the formation of acetophenone is observed along with a gradual erosion of the ee. This suggests that the alcohol oxidation is (partially) stereospecific: (*R*)-PhEtOH is oxidized preferentially to acetophenone. Indeed, kinetic resolution of (*rac*)-PhEtOH by $\text{biot}^{\text{C}4}\text{-1}\cdot\text{Sav S112R}$ affords acetophenone (TTON = 38), leaving enantioenriched (*S*)-PhEt (20% ee after 3 h, $E = k_{(\text{R})}/k_{(\text{S})} = 3.4$, Figure S9).

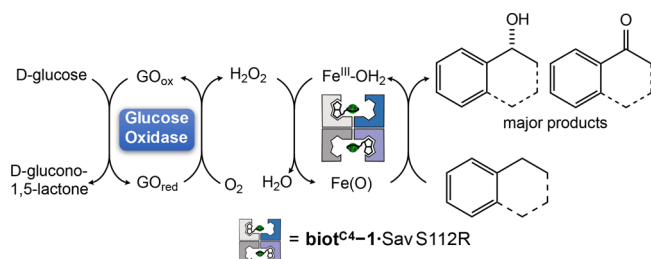
In contrast, product analysis after PhEt oxidation by $\text{biot}^{\text{C}4}\text{-1}\cdot\text{Sav}$ (Sav: K121R or S112R/K121E) yielded ee of (*S*)-PhEtOH (Scheme 2), the opposite enantiomer than $\text{biot}^{\text{C}4}\text{-1}\cdot\text{Sav S112R}$. However, monitoring product formation over time reveals a similar reaction pathway for all three ArMs: The

Scheme 3. Enantioselective Hydroxylation of Tetralin and Kinetic Resolution of Tetralol by $\text{biot}^{\text{C}4}\text{-1}\cdot\text{Sav S112R}$: (a) Consecutive Oxidation Scheme; (b) Time Course of Tetralin Oxidation (Inset: Kinetic Resolution Affords >98% ee (*R*)-Tetralol and TTON = 300); (c) Time Course of the Kinetic Resolution of *rac*-Tetralol by $\text{biot}^{\text{C}4}\text{-1}\cdot\text{Sav S112R}$ (Inset: Kinetic Resolution Yields >99% ee (*R*)-Tetralol (TTON = 220); See SI for Details)

hydroxylation of PhEt yields preferentially (*R*)-PhEtOH, which is then oxidized faster to acetophenone (Figures S10–S11). This mechanistic pathway is reflected in an erosion of ee over time, eventually affording (*S*)-PhEtOH with both Sav K121R and Sav S112R/K121E. Indeed, the ee is highly variable, depending on conversion and mutant.

The reaction conditions to improve the performance of the hydroxylase were fine-tuned for $\text{biot}^{\text{C}4}\text{-1}\cdot\text{Sav S112R}$. A large excess of H₂O₂ favors overoxidation and erosion of ee (Figure S13). The impact of Sav on the activity is also evident at different pH's: $\text{biot}^{\text{C}4}\text{-1}\cdot\text{Sav S112R}$ displays maximum TTON

Scheme 4. Cascade with GO To Generate H₂O₂ *in Situ*, Enabling Hydroxylation Using O₂ as Oxidant^a



^aSee SI.

and enantioselectivity at $8.2 < \text{pH} < 8.8$. Outside this window, the activity decreases markedly (Figure S14). The free cofactor **biot^{C4}-1** has maximum activity at $6 < \text{pH} < 8$ and is quenched at higher pH.

Structural Characterization. To scrutinize the differences in the second coordination sphere that influence the activity of the ArMs, we determined their structure by crystallography. Data sets were obtained for **biot^{C4}-1-Sav** and **biot^{C5}-1-Sav** (Sav = WT, S112R, and S112R/K121E, Tables S1 and S2).

The structures reveal the following features: all six structures are nearly superimposable, reflected by a C _{α} -RMSD varying between 0.038 and 0.256 Å (Table S3). The electron density of the Fe-TAML moiety is defined for **biotC4-1**; the Fe-occupancy is 60% for Sav WT and 100% for Sav S112R and S112R/K121E (Figure 1). This contrasts with **biotC5-1**, for which only the electron density of the biotin C5-linker is defined and modeled with 100% occupancy (Figures S5–S7). We tentatively trace this to the higher flexibility of the C5-linker, resulting in delocalization of the Fe-TAML moiety.

The localization of the Fe(TAML) moiety is affected by the residue at position 112 (Figures 1 and S2–S4). For **biot^{C4}-1-Sav** WT, the closest amino acids, are Sav^A S112 (3.7 Å) and Sav^B K121' (4.2 Å). They hardly interact with Fe(TAML), resulting in a reduced occupancy of Fe(TAML). The mutation Sav S112R forces the Fe(TAML) into a fixed conformation with 100% occupancy, placing the arginine within H-bonding distance to the C=O of the Fe(TAML) (2.5 Å, in one of two conformations, Figure 1b). This alternative position of Fe(TAML) allows Sav^B K121' to coordinate to Fe of **biot^{C4}-1-Sav^A** (2.3 Å, Figure 1b). To enable the coordination of Sav^B K121' to the Fe of **biot^{C4}-1**, the lysine side chain adopts a compact conformation with acute dihedral (χ) angles of 54.2°, 106.9°, 80.0°, and 41.2°. We hypothesize that both the precise localization of the Fe(TAML) and its interaction with either K121' or E121' through an η^2 -coordination (in **biot^{C4}-1-Sav** S112R/K121E, Fe...O 2.3 and 2.9 Å, Figure 1c) impact the catalysis outcome (product distribution and ee, Scheme 2).

Substrate Scope. The substrate scope for **biot^{C4}-1-Sav** S112R was expanded to substrates containing benzylic C(sp³)-H bonds (Table 1). Propylbenzene and butylbenzene afforded the corresponding (*R*)-alcohol in 45% ee (TTON = 26 and 19, respectively). Electron-rich *p*-substituted ethylbenzenes afforded higher TTONs, highlighting the electrophilic character of the Fe(O) species (Figure S15).

A kinetic isotope effect KIE = 9.2 was determined for the oxidation of PhEt/PhEt-*d*₁₀ by **biot^{C4}-1-Sav** S112R at 25 °C (Figure S16). This value compares well with the previously described KIE for Fe-TAML complexes and suggests that the

rate-determining step of the reaction is the hydrogen abstraction.^{56,60,67,68}

The oxidation of indane and tetralin (BDE_{C-H} = 87 and 85.7 kcal/mol)⁶⁹ afforded high TTONs (TTON = 205 and 316, respectively) and good ee in favor of the (*R*)-alcohol (47% and 65% ee, respectively, Table 1).

Prompted by the good TTON and ee for tetralin, its oxidation by **biot^{C4}-1-Sav** S112R was scrutinized. Using 2.5 equivalents of H₂O₂, 73% ee of (*R*)-tetralol was determined at early stages (Scheme 3a). In contrast to PhEt oxidation, the ee increased with conversion, highlighting the preferential (over)-oxidation of (*S*)-tetralol. After 3 h, >98% ee (*R*)-tetralol was obtained (TTON = 300, Scheme 3b). Minimal overoxidation at the second benzylic position was also detected (Figure S17). Oxidation of (*rac*)-tetralol with **biot^{C4}-1-Sav** S112R yielded tetralone and >99% ee of (*R*)-tetralol (unreacted starting material) after ~120 min (Scheme 3c, $E = k_{(S)}/k_{(R)} = 2.7$, and Figure S18). Similarly, a TTON of 173 was obtained for indane oxidation (80% ee (*R*)-indanol, Figure S19). Thus, (*R*)-benzyl-alcohol derivatives are preferentially overoxidized, while the (*S*)-enantiomers of the cyclic derivatives (tetralol and indanol) are oxidized faster. This phenomenon can be attributed to the 1,3-allylic strain (Scheme S2).^{70,71}

Lastly, we developed an enzymatic cascade with Glucose Oxidase (GO) to enable the *in situ* production of H₂O₂, using O₂ as oxidant and glucose as reductant (Scheme 4).⁷² To our delight, after combining **biot^{C4}-1-Sav** S112R and GO the oxidation reactions progressed in a similar way compared to the single batch addition of H₂O₂. A TTON of 50 was obtained for PhEt oxidation, with an initial ee of (*R*)-PhEtOH of 47%, which eroded to 37% after kinetic resolution. For tetralin, a TTON of 170 was obtained, again observing the initial formation of (*R*)-tetralol in 64% ee and posterior kinetic resolution that upgraded it to up to 95%.

Catalysts derived from earth-abundant metals are gaining attention in homogeneous catalysis. The inherent lability of most such systems however limits their use in water. In contrast to polypyridinamine-derived catalysts,⁷³ and thanks to its remarkable stability and catalytic activity, the Fe(TAML) system proved amenable to the design and optimization of an artificial hydroxylase based on the biotin–streptavidin technology.

Chemogenetic optimization of the catalytic performance led to the identification of **biot^{C4}-1-Sav** S112R as our best hydroxylase for the oxidation of benzylic C–H bonds. With *in vivo* applications in mind, we have shown that the activity of the artificial hydroxylase is compatible with glucose oxidase, using O₂ as the terminal oxidant.

Efforts at modulating the activity of the hydroxylase by fine-tuning the cofactors' structure, and expanding the substrate scope toward the oxidation of more complex molecules, are currently underway.

■ ASSOCIATED CONTENT

Supporting Information

The Supporting Information is available free of charge at <https://pubs.acs.org/doi/10.1021/jacs.0c02788>.

General information, experimental section, Figures S1–S21, Tables S1–S6, Scheme S1–S2 (PDF)

■ AUTHOR INFORMATION

Corresponding Author

Thomas R. Ward – Department of Chemistry, University of Basel, CH-4058 Basel, Switzerland; orcid.org/0000-0001-8602-5468; Email: thomas.ward@unibas.ch

Authors

Joan Serrano-Plana – Department of Chemistry, University of Basel, CH-4058 Basel, Switzerland; orcid.org/0000-0003-2735-0943

Corentin Rumo – Department of Chemistry, University of Basel, CH-4058 Basel, Switzerland; orcid.org/0000-0001-7411-5212

Johannes G. Rebelein – Department of Chemistry, University of Basel, CH-4058 Basel, Switzerland; orcid.org/0000-0003-2560-716X

Ryan L. Peterson – Department of Chemistry, University of Basel, CH-4058 Basel, Switzerland; Department of Chemistry and Biochemistry, Texas State University, 78666, Texas, United States; orcid.org/0000-0002-9654-703X

Maxime Barnet – Department of Chemistry, University of Basel, CH-4058 Basel, Switzerland

Complete contact information is available at:
<https://pubs.acs.org/10.1021/jacs.0c02788>

Notes

The authors declare no competing financial interest.

■ ACKNOWLEDGMENTS

T.R.W. thanks the University of Basel, the NCCR Molecular Systems engineering, the SNF (Grant 200020_182046) and the ERC (the DrEAM, Advanced Grant 694424). J.S.-P. thanks the EU for a Marie Skłodowska-Curie fellowship (H2020-MSCA-IF-2016). J.G.R. thanks the European Molecular Biology Organisation for a long-term fellowship (EMBO ALTF 194-2017).

■ REFERENCES

- (1) Hartwig, J. F.; Larsen, M. A. Undirected, Homogeneous C–H Bond Functionalization: Challenges and Opportunities. *ACS Cent. Sci.* **2016**, *2*, 281–292.
- (2) Bergman, R. G. C–H activation. *Nature* **2007**, *446*, 391–393.
- (3) Ye, B.; Zhao, J.; Zhao, K.; McKenna, J. M.; Toste, F. D. Chiral Diaryliodonium Phosphate Enables Light Driven Diastereoselective α -C(sp³)-H Acetalization. *J. Am. Chem. Soc.* **2018**, *140*, 8350–8356.
- (4) Hartwig, J. F. Evolution of C–H Bond Functionalization from Methane to Methodology. *J. Am. Chem. Soc.* **2016**, *138*, 2–24.
- (5) Wencel-Delord, J.; Glorius, F. C–H bond activation enables the rapid construction and late-stage diversification of functional molecules. *Nat. Chem.* **2013**, *5*, 369–375.
- (6) Labinger, J. A.; Bercaw, J. E. Understanding and exploiting C–H bond activation. *Nature* **2002**, *417*, 507–514.
- (7) Newton, C. G.; Wang, S.-G.; Oliveira, C. C.; Cramer, N. Catalytic Enantioselective Transformations Involving C–H Bond Cleavage by Transition-Metal Complexes. *Chem. Rev.* **2017**, *117*, 8908–8976.
- (8) Costas, M.; Mehn, M. P.; Jensen, M. P.; Que, L. Dioxygen Activation at Mononuclear Nonheme Iron Active Sites: Enzymes, Models, and Intermediates. *Chem. Rev.* **2004**, *104*, 939–986.
- (9) Lewis, J. C.; Coelho, P. S.; Arnold, F. H. Enzymatic functionalization of carbon–hydrogen bonds. *Chem. Soc. Rev.* **2011**, *40*, 2003–2021.
- (10) Ortiz de Montellano, P. R. Hydrocarbon Hydroxylation by Cytochrome P450 Enzymes. *Chem. Rev.* **2010**, *110*, 932–948.

- (11) Adam, W.; Lukacs, Z.; Harmsen, D.; Saha-Möller, C. R.; Schreiber, P. Biocatalytic Asymmetric Hydroxylation of Hydrocarbons with the Topsoil-Microorganism *Bacillus megaterium*. *J. Org. Chem.* **2000**, *65*, 878–882.

- (12) Nam, W. Synthetic Mononuclear Nonheme Iron–Oxygen Intermediates. *Acc. Chem. Res.* **2015**, *48*, 2415–2423.

- (13) Jasniewski, A. J.; Que, L. Dioxygen Activation by Nonheme Diiron Enzymes: Diverse Dioxygen Adducts, High-Valent Intermediates, and Related Model Complexes. *Chem. Rev.* **2018**, *118*, 2554–2592.

- (14) Que, L.; Tolman, W. B. Biologically inspired oxidation catalysis. *Nature* **2008**, *455*, 333–340.

- (15) Bruijninx, P. C. A.; van Koten, G.; Klein Gebbink, R. J. M. Mononuclear non-heme iron enzymes with the 2-His-1-carboxylate facial triad: recent developments in enzymology and modeling studies. *Chem. Soc. Rev.* **2008**, *37*, 2716–2744.

- (16) Battistella, B.; Ray, K. O₂ and H₂O₂ activations at dinuclear Mn and Fe active sites. *Coord. Chem. Rev.* **2020**, *408*, 213176.

- (17) Ray, K.; Pfaff, F. F.; Wang, B.; Nam, W. Status of Reactive Non-Heme Metal–Oxygen Intermediates in Chemical and Enzymatic Reactions. *J. Am. Chem. Soc.* **2014**, *136*, 13942–13958.

- (18) Zheng, C.; You, S.-L. Recent development of direct asymmetric functionalization of inert C–H bonds. *RSC Adv.* **2014**, *4*, 6173–6214.

- (19) Milan, M.; Bietti, M.; Costas, M. Enantioselective aliphatic C–H bond oxidation catalyzed by bioinspired complexes. *Chem. Commun.* **2018**, *54*, 9559–9570.

- (20) Saint-Denis, T. G.; Zhu, R.-Y.; Chen, G.; Wu, Q.-F.; Yu, J.-Q. Enantioselective C(sp³)-H bond activation by chiral transition metal catalysts. *Science* **2018**, *359*, No. eaao4798.

- (21) White, M. C.; Zhao, J. Aliphatic C–H Oxidations for Late-Stage Functionalization. *J. Am. Chem. Soc.* **2018**, *140*, 13988–14009.

- (22) Shugrue, C. R.; Miller, S. J. Applications of Nonenzymatic Catalysts to the Alteration of Natural Products. *Chem. Rev.* **2017**, *117*, 11894–11951.

- (23) Groves, J. T.; Viski, P. Asymmetric hydroxylation by a chiral iron porphyrin. *J. Am. Chem. Soc.* **1989**, *111*, 8537–8538.

- (24) Frost, J. R.; Huber, S. M.; Breitenlechner, S.; Bannwarth, C.; Bach, T. Enantioselective C–H Oxygenation Catalyzed by a Supramolecular Ruthenium Complex. *Angew. Chem., Int. Ed.* **2014**, *54*, 691–695.

- (25) Burg, F.; Gicquel, M.; Breitenlechner, S.; Pöthig, A.; Bach, T. Site- and Enantioselective C–H Oxygenation Catalyzed by a Chiral Manganese Porphyrin Complex with a Remote Binding Site. *Angew. Chem., Int. Ed.* **2018**, *57*, 2953–2957.

- (26) Murahashi, S.-I.; Noji, S.; Komiyama, N. Catalytic Enantioselective Oxidation of Alkanes and Alkenes Using (Salen)Manganese Complexes Bearing a Chiral Binaphthyl Strapping Unit. *Adv. Synth. Catal.* **2004**, *346*, 195–198.

- (27) Srouf, H.; Maux, P. L.; Simonneaux, G. Enantioselective Manganese-Porphyrin-Catalyzed Epoxidation and C–H Hydroxylation with Hydrogen Peroxide in Water/Methanol Solutions. *Inorg. Chem.* **2012**, *51*, 5850–5856.

- (28) Komiyama, N.; Noji, S.; Murahashi, S.-I. Manganese catalyzed asymmetric oxidation of alkanes to optically active ketones bearing asymmetric center at the α -position. *Tetrahedron Lett.* **1998**, *39*, 7921–7924.

- (29) Milan, M.; Bietti, M.; Costas, M. Highly Enantioselective Oxidation of Nonactivated Aliphatic C–H Bonds with Hydrogen Peroxide Catalyzed by Manganese Complexes. *ACS Cent. Sci.* **2017**, *3*, 196–204.

- (30) Hamada, T.; Irie, R.; Mihara, J.; Hamachi, K.; Katsuki, T. Highly enantioselective benzylic hydroxylation with concave type of (salen)manganese(III) complex. *Tetrahedron* **1998**, *54*, 10017–10028.

- (31) Olivo, G.; Farinelli, G.; Barbieri, A.; Lanzalunga, O.; Di Stefano, S.; Costas, M. Supramolecular Recognition Allows Remote, Site-Selective C–H Oxidation of Methylenic Sites in Linear Amines. *Angew. Chem., Int. Ed.* **2017**, *56*, 16347–16351.

- (32) Gormisky, P. E.; White, M. C. Catalyst-Controlled Aliphatic C–H Oxidations with a Predictive Model for Site-Selectivity. *J. Am. Chem. Soc.* **2013**, *135*, 14052–14055.
- (33) Chen, M. S.; White, M. C. A Predictably Selective Aliphatic C–H Oxidation Reaction for Complex Molecule Synthesis. *Science* **2007**, *318*, 783–787.
- (34) Schwizer, F.; Okamoto, Y.; Heinisch, T.; Gu, Y.; Pellizzoni, M. M.; Lebrun, V.; Reuter, R.; Köhler, V.; Lewis, J. C.; Ward, T. R. Artificial Metalloenzymes: Reaction Scope and Optimization Strategies. *Chem. Rev.* **2018**, *118*, 142–231.
- (35) Pàmies, O.; Diéguez, M.; Bäckvall, J.-E. Artificial Metalloenzymes in Asymmetric Catalysis: Key Developments and Future Directions. *Adv. Synth. Catal.* **2015**, *357*, 1567–1586.
- (36) Upp, D. M.; Lewis, J. C. Selective C–H bond functionalization using repurposed or artificial metalloenzymes. *Curr. Opin. Chem. Biol.* **2017**, *37*, 48–55.
- (37) Perez-Rizquez, C.; Rodriguez-Otero, A.; Palomo, J. M. Combining enzymes and organometallic complexes: novel artificial metalloenzymes and hybrid systems for C–H activation chemistry. *Org. Biomol. Chem.* **2019**, *17*, 7114–7123.
- (38) Davis, H. J.; Ward, T. R. Artificial Metalloenzymes: Challenges and Opportunities. *ACS Cent. Sci.* **2019**, *5*, 1120–1136.
- (39) Lewis, J. C. Artificial Metalloenzymes and Metallopeptide Catalysts for Organic Synthesis. *ACS Catal.* **2013**, *3*, 2954–2975.
- (40) Monnard, F. W.; Nogueira, E. S.; Heinisch, T.; Schirmer, T.; Ward, T. R. Human carbonic anhydrase II as host protein for the creation of artificial metalloenzymes: the asymmetric transfer hydrogenation of imines. *Chem. Sci.* **2013**, *4*, 3269–3274.
- (41) Oohora, K.; Onoda, A.; Hayashi, T. Hemoproteins Reconstituted with Artificial Metal Complexes as Biohybrid Catalysts. *Acc. Chem. Res.* **2019**, *52*, 945–954.
- (42) Mirts, E. N.; Petrik, I. D.; Hosseinzadeh, P.; Nilges, M. J.; Lu, Y. A designed heme-[4Fe-4S] metalloenzyme catalyzes sulfite reduction like the native enzyme. *Science* **2018**, *361*, 1098–1101.
- (43) Lewis, J. C. Beyond the Second Coordination Sphere: Engineering Dirhodium Artificial Metalloenzymes To Enable Protein Control of Transition Metal Catalysis. *Acc. Chem. Res.* **2019**, *52*, 576–584.
- (44) Roelfes, G. LmrR: A Privileged Scaffold for Artificial Metalloenzymes. *Acc. Chem. Res.* **2019**, *52*, 545–556.
- (45) Chino, M.; Maglio, O.; Natri, F.; Pavone, V.; DeGrado, W. F.; Lombardi, A. Artificial Diiron Enzymes with a De Novo Designed Four-Helix Bundle Structure. *Eur. J. Inorg. Chem.* **2015**, *2015*, 3371–3390.
- (46) Lombardi, A.; Pirro, F.; Maglio, O.; Chino, M.; DeGrado, W. F. De Novo Design of Four-Helix Bundle Metalloproteins: One Scaffold, Diverse Reactivities. *Acc. Chem. Res.* **2019**, *52*, 1148–1159.
- (47) Grimm, A. R.; Sauer, D. F.; Polen, T.; Zhu, L.; Hayashi, T.; Okuda, J.; Schwaneberg, U. A Whole Cell E. Coli Display Platform for Artificial Metalloenzymes: Poly(phenylacetylene) Production with a Rhodium–Nitrobindin Metalloprotein. *ACS Catal.* **2018**, *8*, 2611–2614.
- (48) Heinisch, T.; Ward, T. R. Artificial Metalloenzymes Based on the Biotin–Streptavidin Technology: Challenges and Opportunities. *Acc. Chem. Res.* **2016**, *49*, 1711–1721.
- (49) Liang, A. D.; Serrano-Plana, J.; Peterson, R. L.; Ward, T. R. Artificial Metalloenzymes Based on the Biotin–Streptavidin Technology: Enzymatic Cascades and Directed Evolution. *Acc. Chem. Res.* **2019**, *52*, 585–595.
- (50) Wilson, M. E.; Whitesides, G. M. Conversion of a protein to a homogeneous asymmetric hydrogenation catalyst by site-specific modification with a diphosphinerhodium(I) moiety. *J. Am. Chem. Soc.* **1978**, *100*, 306–307.
- (51) Oohora, K.; Kihira, Y.; Mizohata, E.; Inoue, T.; Hayashi, T. C(sp³)–H Bond Hydroxylation Catalyzed by Myoglobin Reconstituted with Manganese Porphycene. *J. Am. Chem. Soc.* **2013**, *135*, 17282–17285.
- (52) Kille, S.; Zilly, F. E.; Acevedo, J. P.; Reetz, M. T. Regio- and stereoselectivity of P450-catalysed hydroxylation of steroids controlled by laboratory evolution. *Nat. Chem.* **2011**, *3*, 738–743.
- (53) Zhang, K.; Shafer, B. M.; Demars, M. D.; Stern, H. A.; Fasan, R. Controlled Oxidation of Remote sp³ C–H Bonds in Artemisinin via P450 Catalysts with Fine-Tuned Regio- and Stereoselectivity. *J. Am. Chem. Soc.* **2012**, *134*, 18695–18704.
- (54) Peters, M. W.; Meinhold, P.; Glieder, A.; Arnold, F. H. Regio- and Enantioselective Alkane Hydroxylation with Engineered Cytochromes P450 BM-3. *J. Am. Chem. Soc.* **2003**, *125*, 13442–13450.
- (55) Collins, T. J. TAML Oxidant Activators: A New Approach to the Activation of Hydrogen Peroxide for Environmentally Significant Problems. *Acc. Chem. Res.* **2002**, *35*, 782–790.
- (56) Collins, T. J.; Ryabov, A. D. Targeting of High-Valent Iron-TAML Activators at Hydrocarbons and Beyond. *Chem. Rev.* **2017**, *117*, 9140–9162.
- (57) Chahbane, N.; Popescu, D.-L.; Mitchell, D. A.; Chanda, A.; Lenoir, D.; Ryabov, A. D.; Schramm, K.-W.; Collins, T. J. FeIII–TAML-catalyzed green oxidative degradation of the azo dye Orange II by H₂O₂ and organic peroxides: products, toxicity, kinetics, and mechanisms. *Green Chem.* **2007**, *9*, 49–57.
- (58) Ryabov, A. D.; Collins, T. J. Mechanistic considerations on the reactivity of green Fe^{III}-TAML activators of peroxides. *Adv. Inorg. Chem.* **2009**, *61*, 471–521.
- (59) Ghosh, M.; Nikhil, Y. L. K.; Dhar, B. B.; Sen Gupta, S. Mechanism of Alcohol Oxidation by Fe^V(O) at Room Temperature. *Inorg. Chem.* **2015**, *54*, 11792–11798.
- (60) Kwon, E.; Cho, K.-B.; Hong, S.; Nam, W. Mechanistic insight into the hydroxylation of alkanes by a nonheme iron(v)–oxo complex. *Chem. Commun.* **2014**, *50*, 5572–5575.
- (61) Napoly, F.; Kieffer, R.; Jean-Gérard, L.; Goux-Henry, C.; Draye, M.; Andrioletti, B. Fe(TAML)Li/tert-butyl hydroperoxide as a new combination for benzylic C–H oxidation. *Tetrahedron Lett.* **2015**, *56*, 2517–2520.
- (62) Das, A.; Nutting, J. E.; Stahl, S. S. Electrochemical C–H oxygenation and alcohol dehydrogenation involving Fe-oxo species using water as the oxygen source. *Chem. Sci.* **2019**, *10*, 7542–7548.
- (63) Dundas, C. M.; Demonte, D.; Park, S. Streptavidin–biotin technology: improvements and innovations in chemical and biological applications. *Appl. Microbiol. Biotechnol.* **2013**, *97*, 9343–9353.
- (64) Ren, Q.; Guo, Y.; Mills, M. R.; Ryabov, A. D.; Collins, T. J. On the Iron(V) Reactivity of an Aggressive Tail-Fluorinated Tetraamido Macrocyclic Ligand (TAML) Activator. *Eur. J. Inorg. Chem.* **2015**, *2015*, 1445–1452.
- (65) Acetone was selected as cosolvent to ensure dissolution of the substrates. Its presence influences the product distribution by diminishing alcohol oxidation. See SI for more details.
- (66) TTON refers to the total turnover number and includes the C–H hydroxylation and alcohol oxidation products, quantified by GC-FID. See SI for more details.
- (67) Ghosh, M.; Singh, K. K.; Panda, C.; Weitz, A.; Hendrich, M. P.; Collins, T. J.; Dhar, B. B.; Sen Gupta, S. Formation of a Room Temperature Stable Fe^V(O) Complex: Reactivity Toward Unactivated C–H Bonds. *J. Am. Chem. Soc.* **2014**, *136*, 9524–9527.
- (68) Kundu, S.; Thompson, J. V. K.; Shen, L. Q.; Mills, M. R.; Bominaar, E. L.; Ryabov, A. D.; Collins, T. J. Activation Parameters as Mechanistic Probes in the TAML Iron(V)–Oxo Oxidations of Hydrocarbons. *Chem. - Eur. J.* **2015**, *21*, 1803–1810.
- (69) St. John, P. C.; Guan, Y.; Kim, Y.; Kim, S.; Paton, R. S. Prediction of organic homolytic bond dissociation enthalpies at near chemical accuracy with sub-second computational cost. *Nat. Commun.* **2020**, *11*, 2328.
- (70) Hoffmann, R. W. Allylic 1,3-strain as a controlling factor in stereoselective transformations. *Chem. Rev.* **1989**, *89*, 1841–1860.
- (71) Shin-ya, K.; Sugeta, H.; Shin, S.; Hamada, Y.; Katsumoto, Y.; Ohno, K. Absolute Configuration and Conformation Analysis of 1-Phenylethanol by Matrix-Isolation Infrared and Vibrational Circular Dichroism Spectroscopy Combined with Density Functional Theory Calculation. *J. Phys. Chem. A* **2007**, *111*, 8598–8605.

(72) Miller, J. A.; Alexander, L.; Mori, D. I.; Ryabov, A. D.; Collins, T. J. In situ enzymatic generation of H_2O_2 from O_2 for use in oxidative bleaching and catalysis by TAML activators. *New J. Chem.* **2013**, *37*, 3488–3495.

(73) Doble, M. V.; Jarvis, A. G.; Ward, A. C. C.; Colburn, J. D.; Götze, J. P.; Bühl, M.; Kamer, P. C. J. Artificial Metalloenzymes as Catalysts for Oxidative Lignin Degradation. *ACS Sustainable Chem. Eng.* **2018**, *6*, 15100–15107.